Arabian Journal of Chemistry (2022) **15**, 103706

King Saud University

Arabian Journal of Chemistry

www.ksu.edu.sa
www.sciencedirect.com

ORIGINAL ARTICLE

Synthesis, characterization, and challenges faced during the preparation of zirconium pillared clays

Tanya Chauhan [a,b], Mahitha Udayakumar [a,b], Mohammed Ahmed Shehab [a,b], Ferenc Kristály [c], Anett Katalin Leskó [d], Martin Ek [e], David Wahlqvist [e], Pál Tóth [d], Klara Hernadi [f], Zoltán Németh [a,*]

[a] *Advanced Materials and Intelligent Technologies Higher Education and Industrial Cooperation Centre, University of Miskolc, H-3515 Miskolc, Hungary*
[b] *Faculty of Materials Science and Engineering, University of Miskolc, H-3515 Miskolc, Hungary*
[c] *Institute of Mineralogy and Geology, University of Miskolc, H-3515 Miskolc, Hungary*
[d] *Institute of Energy and Quality Affairs, University of Miskolc, H-3515 Miskolc, Hungary*
[e] *Lund University, Centre for Analysis and Synthesis and Nano Lund, Box 124, 22100 Lund, Sweden*
[f] *Institute of Physical Metallurgy, Metal Forming and Nanotechnology, University of Miskolc, H-3515 Miskolc, Hungary*

Received 12 November 2021; accepted 16 January 2022
Available online 21 January 2022

KEYWORDS

Montmorillonite;
Zr-PILCs;
Pillaring;
Sodium-saturated montmorillonite;
Specific surface area;
Basal spacing

Abstract In this study, Zr-pillared montmorillonite clays (Zr-PILCs) were synthesized using two different precursor materials: raw montmorillonite (CM) and sodium ion-saturated montmorillonite (Na-CM) at different Zr/clay ratios (2.5, 5 and 10 mmol/g). To study the effect of Zr concentration and clay pre-treatment with NaCl on pillaring, the modified clay samples were characterized in detail using X-ray diffraction (XRD), Fourier transform infrared spectroscopy (FT-IR), thermogravimetric analysis (TGA), high-resolution transmission electron microscopy (HRTEM), scanning transmission electron microscopy and energy-dispersive X-ray spectroscopy (STEM-EDX). The XRD analysis showed the increase of basal spacing of Zr-PILCs prepared from both precursor materials: from 1.26 to 1.74 nm in the case of CM, and from 1.13 to 1.93 nm for Na-CM. Results from FT-IR revealed new bands ascribed to Zr-O bonds in the range of 400–500 cm^{-1} in Zr-pillared samples obtained from Na-CM at Zr/clay ratios of 2.5 and 5 mmol/g. The distribution and nature of Zr species in between the silicate layers were studied using STEM-EDX and HAADF imaging. They were found to be separated by a distance of 1.5–3 nm and their thickness lies in the range of 1–2 nm. Pillared clays prepared from pre-treatment with NaCl were more thermally stable at higher temperatures.

* Corresponding author.
E-mail address: kemnemet@uni-miskolc.hu (Z. Németh).
Peer review under responsibility of King Saud University.

Production and hosting by Elsevier

1. Introduction

Synthesis of inorganic pillared clays was first reported in the late 1970s (Brindley and Sempels, 1977; Vaughan et al., 1979) by exchanging the charge compensating cations present in the interlayer space of clay

https://doi.org/10.1016/j.arabjc.2022.103706
1878-5352

minerals with bulky polyhydroxy metal cations. Upon further heat treatment, these hydroxy metal cations are converted into metal oxide pillars because of dehydration and dehydroxylation. Oxide pillars keep the clay sheets apart giving them stability, introducing microporosity and surface acidity to the layered material. These newly formed microporous clay structures referred to as pillared interlayered clays (PILCs) are being of great importance due to their excellent adsorption and catalytic properties (Gil and Vicente, 2020). Synthesis of pillared clays involves four main steps; starting with preparation and ageing of the pillaring solution followed by intercalation, washing and calcination (Bergaya et al., 2006). During the ageing of the pillaring solution, polymerization of multivalent cations (such as Al^{3+}, Zr^{4+}, Ti^{4+}, Cr^{3+}, Fe^{3+}) (Gil et al., 2011) takes place and polycations of respective metals are formed, which is followed by the intercalation of these polycations into the clay sheets. The intercalation reaction requires a particular time and temperature. After this, the clay is separated from the solution and washed thoroughly to remove the precursor anions (e.g., Cl^-) as they prevent the homogenous distribution of oxide pillars in the clay structure. The final step is calcination, during which polycations transforms into stable metal oxide clusters referred to as pillars.

Many researchers are working on the synthesis of PILCs and their application for different purposes like adsorption of nutrients, heavy metals, pharmaceutical and personal care products from water (Chauhan et al., 2020). For the preparation of PILCs, the precursor material is very important: smectite is typically used because of its 2:1 layer type structure, in which one alumina octahedral sheet is sandwiched between two silica tetrahedral sheets (Uddin, 2017). The bonding between the two silicate sheets is very weak which permits water and exchangeable ions to enter. This leads to a large swelling capacity. Smectite is regarded as a general term referring to a group of minerals including montmorillonite, nontronite, saponite and hectorite (T. Zhang et al., 2020). Montmorillonite is one of the important members of the smectite group of clay minerals and is commonly used due to its wide abundance, high cation exchange capacity, low cost, large specific surface area and flexible structural properties. The surface of the montmorillonite clay is negatively charged due to the isomorphous substitution of Mg^{2+} for Al^{3+} in the octahedral layer and Al^{3+} for Si^{4+} in the tetrahedral layer, which is balanced by the presence of small exchangeable cations such as Na^+ and Ca^{2+} present in between the clay sheet (Lin et al., 2018). A major drawback of smectite is, during dehydration (heating) the layered structure start decomposing and the intermediate space is no longer accessible for chemical reactions (Najafi et al., 2021). To avoid this problem, pillaring is done which impart permanent porosity to the clay structures.

The concept of intercalation or pillaring was given by Barrer and Mcleod in the 1950s by exchanging inorganic cations of montmorillonite with tetra alkyl ammonium species (Barrer and Macleod, 1955). But the use of organic cations for pillaring was limited due to their low thermal stability - only up to 250 °C. In late 1977, Brindley and Sempels intercalated the hydrolysis product of $AlCl_3$ in sodium saturated beidellite. After aluminium, zirconium polyhydroxy cations were used as pillaring material by Yamanaka and Brindley in 1979 (Yamanaka, 1979). Coordination compounds, organometallic complexes, surfactants, and polymers were also used as pillaring agents by many researchers. But, the most useful and popular pillaring species used so far are polyoxocations as they give high thermal stability to the clays (Gand et al., 2000). In 1988, Vaughan achieved pillaring by using cationic polymers of Al, Zr and Ti with specific surface area and basal spacing of 300 m^2/g and 1.8 nm respectively and the pillared structures were stable up to 600 °C. Work on Al-pillared clays is extensively documented in literature because the hydrolysis behaviour of aluminium cations is fully understood. In 1988, Bartley threw light on the solution chemistry of zirconium ions and factors responsible for the successful pillaring of zirconium into the clay structure. Cool and Vasant also emphasized the parameters which influence the preparation of zirconium pillaring solution. According to them, zirconyl ion is present as a tetramer in solid zirconium chloride with the formula of $[Zr_4(OH)_8(H_2O)_{16}]^{8+}$. In water, rapid polymerization of tetramer takes place and the solution becomes acidic due to hydrolysis of the tetramer (Cool and Vansant, 1998). The degree of polymerization depends upon the pH, concentration, ageing and heating temperature of the zirconium solution. Intercalation of zirconium species in polymerized form produces a larger surface area with more basal spacing and thermal stability (Burch and Warburton, 1986; Bertella and Pergher, 2017). For the preparation of pillared clays, nature of the parent clay material, concentration of the pillaring solution, intercalation reaction and calcination temperature, ageing, stirring time are all important factors (Valenzuela et al., 2003). For the ion exchange reaction, the parent clay can be used in powder form or suspension form. In dilute suspension, expansion of clay sheet takes place which further facilitates the entry of polyhydroxy cation into the clay structure. By adjusting the operating parameters, the structural and surface properties of pillared materials can be tuned.

The parent clay contains many small exchangeable cations such as Mg^{2+}, Na^+, Ca^{2+}. To get a homogeneous structure, the interlayer space can be saturated with one such ion either by acid treatment or with NaCl. Ghnimia and Srasra used sodium saturated bentonite for the preparation of Zr-pillared clays with a metal/clay ratio of 10 mmol/g. They obtained a specific surface area of 199 m^2/g with a basal spacing of 1.82 nm (Mnasri-ghnimi and Frini-srasra, 2019). Lin et al., studied the effect of calcium and sodium ions pretreatment on the adsorption of phosphates on zirconium modified bentonites. It was found that pillared clays prepared from Ca^{2+}-bentonite show better adsorption results than Na^+-bentonite. They also had a higher specific surface area (108.4 m^2/g) and total pore volume (0.1163 cm^3/g) (Lin et al., 2018). Yuan et al. prepared Fe-pillared montmorillonite clays by using Ca^{2+}-Mt and Na^+-Mt as precursor material. Na^+ activated montmorillonite was prepared by an ion-exchange reaction between Ca^{2+}-Mt and Na_2CO_3. They observed that pillared clays synthesized from Na^+-Mt show higher specific surface area and porosity than those obtained from Ca^{2+}-Mt. They also concluded that the Na^+ activation process influences the structure of powdered montmorillonite based on the fact that higher basal spacing was obtained in the case of Na^+-Mt than Ca^{2+}-Mt (Yuan et al., 2008).

The objective of this research was to investigate the influence of Na^+ pre-treatment on the process of pillaring. A series of Zr-modified clays were prepared using two precursor materials; naturally occurring montmorillonite (CM) and sodium exchanged montmorillonite (Na-CM) at different Zr/clay ratios i.e. 2.5, 5, 10 mmol/g. A detailed comparative analysis of the prepared materials was done for a better understanding of the nature of zirconium pillars created inside the clay structure. In this work, a novel analysis about the dimensions and distribution of microstructures produced by the pillaring process was made with the help of HRTEM, STEM-EDX and HAADF imaging techniques.

2. Experimental

2.1. Materials

Naturally occurring raw montmorillonite (CM) used in this study was purchased from VWR with the brand name Alfa Aesar. All chemical reagents including zirconium oxychloride octahydrate ($ZrOCl_2{\cdot}8H_2O$ of purity 98%), potassium chloride (KCl), ethanol, sodium chloride (NaCl), silver nitrate ($AgNO_3$), hydrochloric acid (HCl), copper sulphate ($CuSO_4$), Tris (hydroxymethyl) aminomethane, ethylenediamine ($C_2H_8N_2$ of purity 99%) used were analytical grade. Distilled water was used to prepare all the solutions in the experiments.

2.2. Preparation of Zr-PILCs

Zr-pillared clays were synthesized using two precursor materials (CM, Na-CM) at three different Zr/clay ratios (2.5, 5,

10 mmol/g). Na-CM was prepared by saturating raw montmorillonite with 1 M NaCl for 24 h. After saturation, the clay was recovered from the salt solution by centrifugation, washed properly and dried at 60 °C. 0.1 M pillaring solution of $ZrOCl_2 \cdot 8H_2O$ was prepared and aged for 24 h at room temperature. Ageing of zirconium oxychloride solution leads to an increase in the degree of polymerization due to an increase in the rate of hydrolysis. 2 g of montmorillonite clay was dispersed in 200 mL of distilled water to form clay suspension. To ensure proper dispersion and swelling, the clay suspension was stirred at room temperature for 2 h. Then, the Zr pillaring solution was added to the clay suspension dropwise and kept at 50 °C under vigorous stirring. The suspension was left for stirring for 2 h, followed by an ageing of 12 h at 50 °C. Then, the intercalated clay was centrifuged and washed thoroughly. Finally, the modified clay material was dried in a hot air oven at 120 °C. Cation exchange capacity (CEC) of CM (56 $cmol^+/kg$) and Na-CM (52 $cmol/^+kg$) was determined using adsorption of copper ethylenediamine complex, $[Cu(en)_2]^{+2}$ (Ammann, Bergaya, and Lagaly, 2005). The Zr-modified CM and Na-CM were denoted as Zr-50-2.5, Zr-50-5, Zr-50-10 and Na-Zr-50-2.5, Na-Zr-50-5, Na-Zr-50-10, respectively.

2.3. Methods of characterization

X-ray powder diffraction (XRD) measurements were performed with Bruker D8 Advance instrument (Cu-Kα source, 40 kV and 40 mA generator settings) in parallel beam geometry obtained with Göbel mirror and Vantec1 position sensitive detector (1° opening). Measurements were recorded in the 2–70° (2θ) range with 0.007° (2θ)/24 counting time.

The specific surface area was determined by CO_2 adsorption at 273 K using the ASAP 2020 instrument (Micromeritics Instrument Corp. USA). Dubinin Asthakov model was applied for the CO_2 adsorption isotherms. Before making the measurements, the samples were degassed at 90 °C for 24 h.

Thermogravimetric analysis (TGA) was done using the MOM Derivatograph C/PC instrument. Approximately, 100 mg of sample was heated from 25 to 1000 °C at a rate of 5 °C/min under air.

Fourier transform infrared spectroscopy (FTIR, Bruker Vortex 70) was used to investigate the structure, bonding, and chemical properties of clay samples. Measurements were taken in the wavenumber range of 400 to 4000 cm^{-1} with an average of 50 scans and a resolution of 4 cm^{-1}.

High-Resolution Transmission Electron Microscopy (HRTEM) micrographs were obtained using a Hitachi HF3300S environmental transmission electron microscope. Digital micrographs of the clay samples were further analyzed using Fast Fourier Transforms (FFT). An in-house developed, open-source image analysis code was used to measure basal spacing in HRTEM images (Toth, 2021). The thickness and spatial distribution of the Zr-rich domains were further studied in Scanning TEM (STEM) mode using High Angle Annular Dark Field (HAADF) imaging and Energy Dispersive X-ray Spectroscopy (EDX, Oxford Instruments SDD X-Max^N 80T). Non-negative matrix factorization (NMF), described in detail by Muto, 2019) and implemented via the HyperSpy library for python, was used to aid localization of Zr-rich regions in the EDX spectrum images.

3. Results and discussion

The XRD patterns of raw montmorillonite (CM) and its Zr-pillared forms (Zr-50-2.5, Zr-50-5, Zr-50-10) are shown in Fig. 1A. In CM, a sharp diffraction peak appeared at 6.97° corresponding to a basal spacing of 1.26 nm, and a weak peak appeared at 19.82° corresponding to the montmorillonite (Mt) crystal structure. Other distinct diffraction peaks at 21.95°and 26.64° were attributed to impurities of cristobalite and quartz, respectively. In Zr-50-2.5, the intensity of the Mt peak decreased and shifted toward lower 2θ, i.e., 5.08° corresponding to a basal spacing of 1.74 nm. The increase in basal spacing by 0.48 nm implied the intercalation of zirconium polyhydroxy cations into the interlayer space of the clay mineral, however, the decreased peak intensity suggested a degree of aperiodicity in the clay structure. In Zr-50-5, two weak reflections were obtained at 2θ = 5.08°, 8.8° corresponding to d_{001} values of 1.74 and 1 nm, respectively. Weak reflections indicate that the layers of clays were not homogenously spaced. In Zr-50-10, the Mt peak shifted toward 2θ = 8.94°, corresponding to d_{001} = 0.99 nm. The thickness of the silicate layer in montmorillonite is ~1 nm (Zhou et al., 2019) – this means that at higher concentrations of zirconium, the basal spacing decreased and the crystal structure of the clay started collapsing.

The XRD patterns of Na-CM and its Zr-modified forms (Na-Zr-50-2.5, Na-Zr-50-5, Na-Zr-50-10) are shown in Fig. 1B. In Na-CM, a reflection appeared at 2θ = 7.77° with a d_{001} value of 1.13 nm corresponding to the Mt peak. A remarkable shift of the Mt peak toward the lower 2θ value and higher basal plane spacing was observed in the pillared samples. In Na-Zr-50-2.5 and Na-Zr-50-5, well defined Mt peaks were observed at 2θ = 4.84°, 4.76° (d_{001} = 1.82, 1.85 nm), respectively. These d_{001} values matched the literature data (Gand et al., 2000; Zou et al., 2020). The increase in basal spacing by 0.69 and 0.72 nm proves that pillaring was successful in both samples. A split in the peak was observed at 2θ = 4.60 °, 7.37 ° (d_{001} = 1.93, 1.19 nm) in the case of Na-Zr-50-10 which suggested the presence of two fractions of clay with different basal spacing.

Textural properties of the parent clay and their Zr-modified forms are summarized in Table 1. It shows that all the Zr-pillared clay samples exhibit high porosity and increased surface area as compared to the precursor material. The largest surface area (280 m^2/g) was exhibited by Zr-50-2.5, with a micropore volume of 0.143 cm^3/g followed by the sample Na-Zr-50-5 with a specific surface area of 240 m^2/g and a micropore volume of 0.122 cm^3/g.

The FTIR spectra of the parent precursor and the pillared clays are shown in Figs. 2 & 3. In Fig. 2, CM exhibited a band at 3623 cm^{-1} corresponding to the stretching vibration of the O-H bond coordinated with aluminium atoms of the octahedral layer (KouSun et al., 1998). In the pillared samples, this band disappeared. Bands near 3422 cm^{-1} and 1635 cm^{-1} were attributed to the H-O-H stretching and bending vibrations of adsorbed water (Frost et al., 2000; Madejová, 2003). The former band is related to the presence of interlayer water. As an effect of the modification, these bands disappeared in zirconium treated samples. The Si-O stretching vibration was represented in the range of 1200–700 cm^{-1} (KouSun et al., 1998; Zviagina et al., 2020). This band was shifted towards a higher

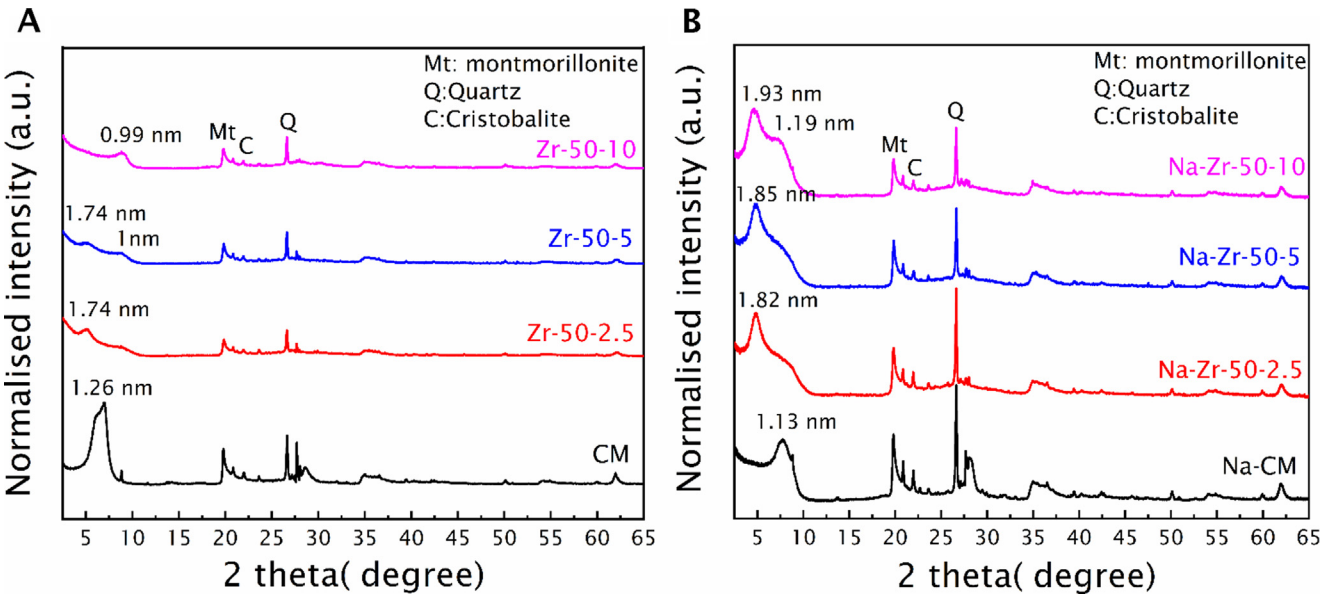

Fig. 1 XRD patterns of raw and Zr pillared montmorillonite **(A)**; and sodium saturated montmorillonite clays **(B)**.

Table 1 Textural properties of precursor and Zr-pillared clays.

Sample	Specific surface area (m^2/g)	Micropore volume (cm^3/g)	Average pore diameter (nm)
CM	40.5	0.021	2.03
Zr-50-2.5	280	0.143	2.04
Zr-50-5	129	0.054	1.7
Zr-50-10	134	0.056	1.67
Na-CM	28.3	0.012	1.75
Na-Zr-50-2.5	216	0.099	1.84
Na- Zr-50-5	240	0.122	2
Na-Zr-50-10	135	0.057	1.7

wavenumber in zirconium treated samples. The bands at 915 cm^{-1} and 846 cm^{-1} originated from the deformation of Al-Al-OH and Al-Mg-OH, respectively (Yuan et al., 2008; Zhou et al., 2010). The intensity of bands between 500 and 1000 cm^{-1} decreased in the Zr-modified samples.

In pillared forms of Na-CM (Na-Zr-50-2.5, Na-Zr-50-5), new bands were identified in the spectral range of 400–500 cm^{-1} (Fig. 3B). In Na-Zr-50-2.5, two new bands were observed at 404 and 418 cm^{-1}. Three new bands at 410, 420 and 442 cm^{-1} appeared in the case of Na-Zr-50-5 (Fig. 3B). These new vibration bands were attributed to the presence of Zr-O bonds (Bačić, 2017; NerisMeireles et al., 2020; Onyango et al., 2007). A possible explanation for this could be when CM was treated with NaCl, sodium ions entered the interlayer space and interlayer water was removed as an

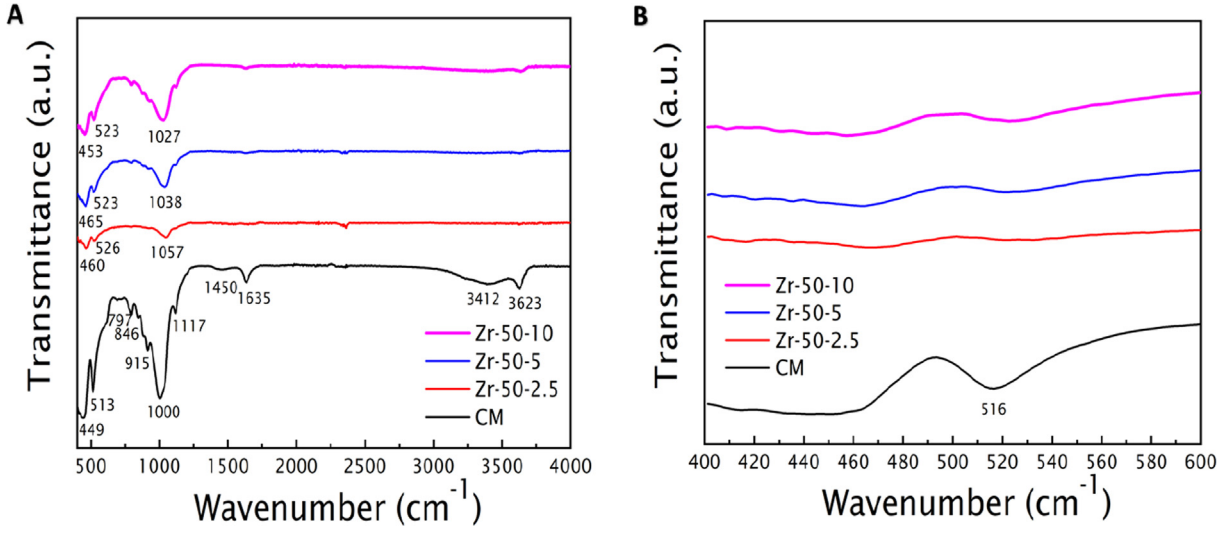

Fig. 2 FTIR spectra of CM and Zr-50-2.5, Zr-50-5 and Zr-50-10 **(A, B)**.

effect of heating. This makes the clay structure homogenized and the sodium ions facilitate the subsequent exchange with zirconium ions. Also, the mobility of the interlayer ions depends on the stability of the hydration shell around them. Sodium ions have a less stable hydration shell therefore they have more mobility. In CM, sodium ions are present along

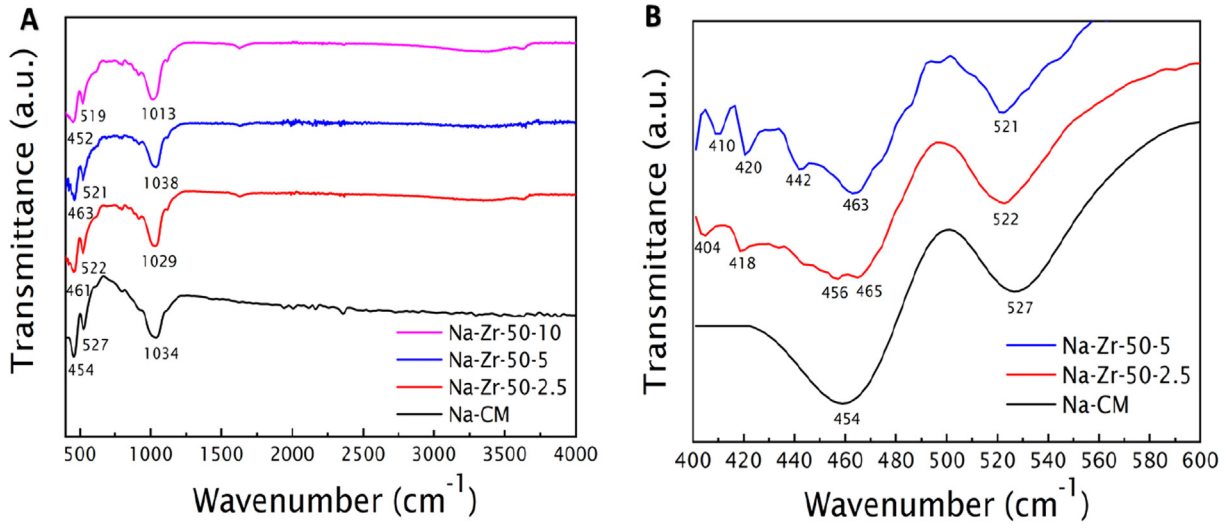

Fig. 3 FTIR spectra of Na-CM and Zr pillared Na-CM **(A, B)**.

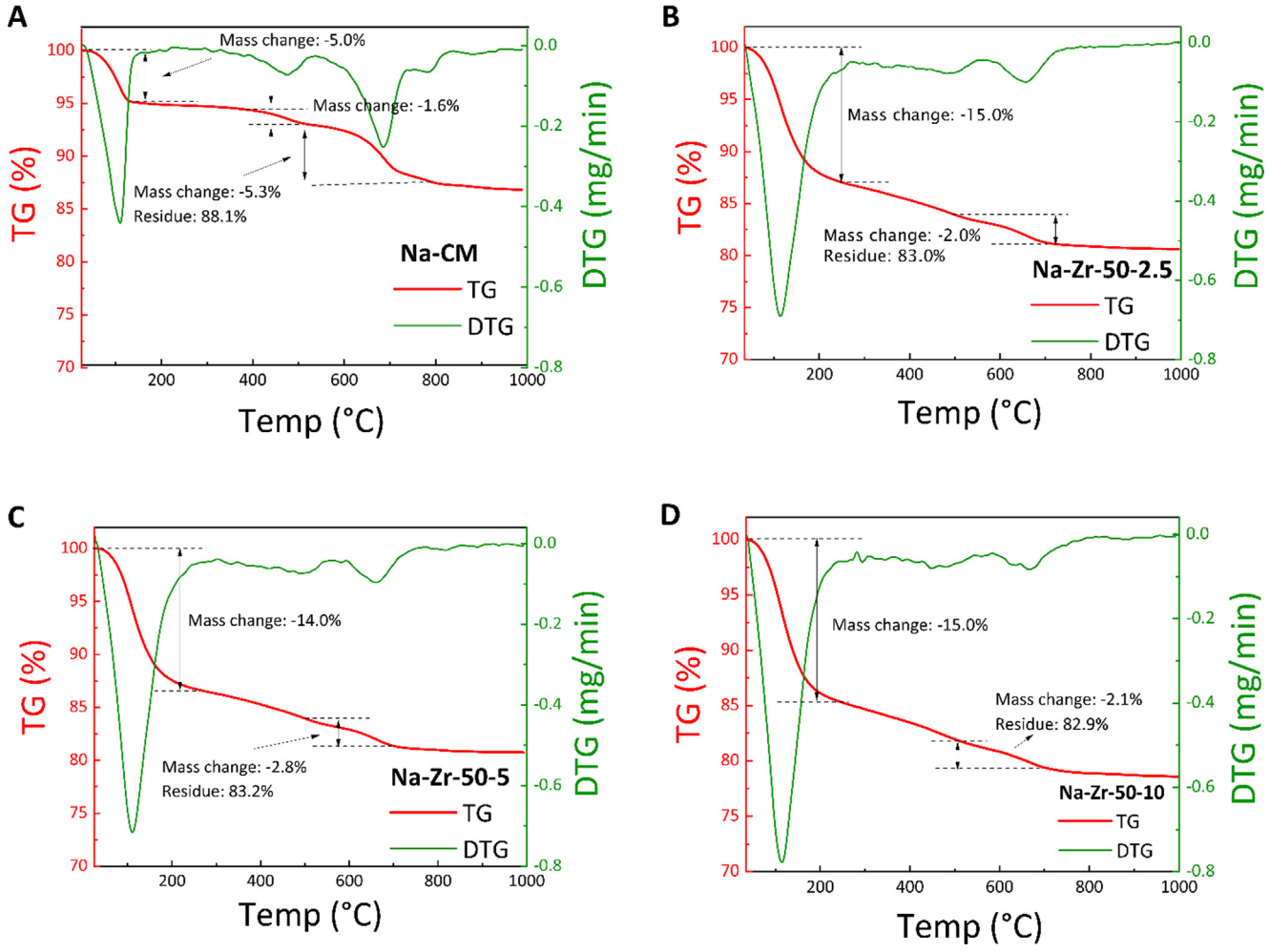

Fig. 4 Thermogravimetric curves of Na-CM **(A)**; Na-Zr-50-2.5 **(B)**; Na-Zr-50-5 **(C)** and Na-Zr-50-10 **(D)**.

with other cations such as calcium and potassium therefore the moving region of Na^+ ions is constrained by the hydration shell of other cations (L. Zhang et al., 2014). The FTIR results supported the XRD results which confirm successful intercalation of zirconium species in between the clay sheets.

The thermogravimetric and the derivative curves are depicted in Fig. 4. The percentage mass loss in the material over a range of temperature is represented by the TG curve; the derivative of which with respect to temperature (DTG) was used to study the steps of thermal transformation. In Fig. 4, the thermogravimetric curves of Na-CM and pillared clay samples show that the stability of clay structure increased after pillaring. This can be attributed to the fact that during the process of pillaring, stable metal oxide pillars are formed between the silicate sheets that impart rigidity to the clay structure. Previous studies revealed that the thermal decomposition of clay takes place in two steps: in the range of 35–150 °C, physically adsorbed water is lost, and in 450–800 °C, dehydroxylation of silicate structure takes place (Baloyi et al., 2019; Chae et al., 2001). In consistence with this, the first step of thermal decomposition could be seen between 25 and 110 °C, while the second step was observed between 400 and 800 °C. Pillared samples exhibited higher relative mass loss than Na-CM at lower temperature and lower mass loss at a higher temperature corresponding to removal of hydroxyl groups from the internal and external surface of the PILCS. In the case of Zr-modified samples, additional mass loss in the first step can be expected due to zirconium species. In the case of CM and its pillared forms, similar results were obtained which is shown in Fig. S1 provided in the supplementary document.

The nature of the ZrO_2-pillaring and intercalation was further investigated using STEM-HAADF imaging and EDX spectroscopy. A comparison of a HAADF image and the Zr-rich component from the corresponding EDX spectrum image (Fig. 5A and B), acquired in a viewing direction parallel to the clay basal planes, reveals that the bright areas in the former can be ascribed to intercalated ZrO_2. This interpretation is also supported by the high HAADF-intensity of these areas, which stems from the much larger atomic number of Zr compared to the other elements present in the clay. Higher-resolution HAADF images (Fig. 5D, E) display thin Zr-rich layers evenly distributed throughout the material. Due to this very even

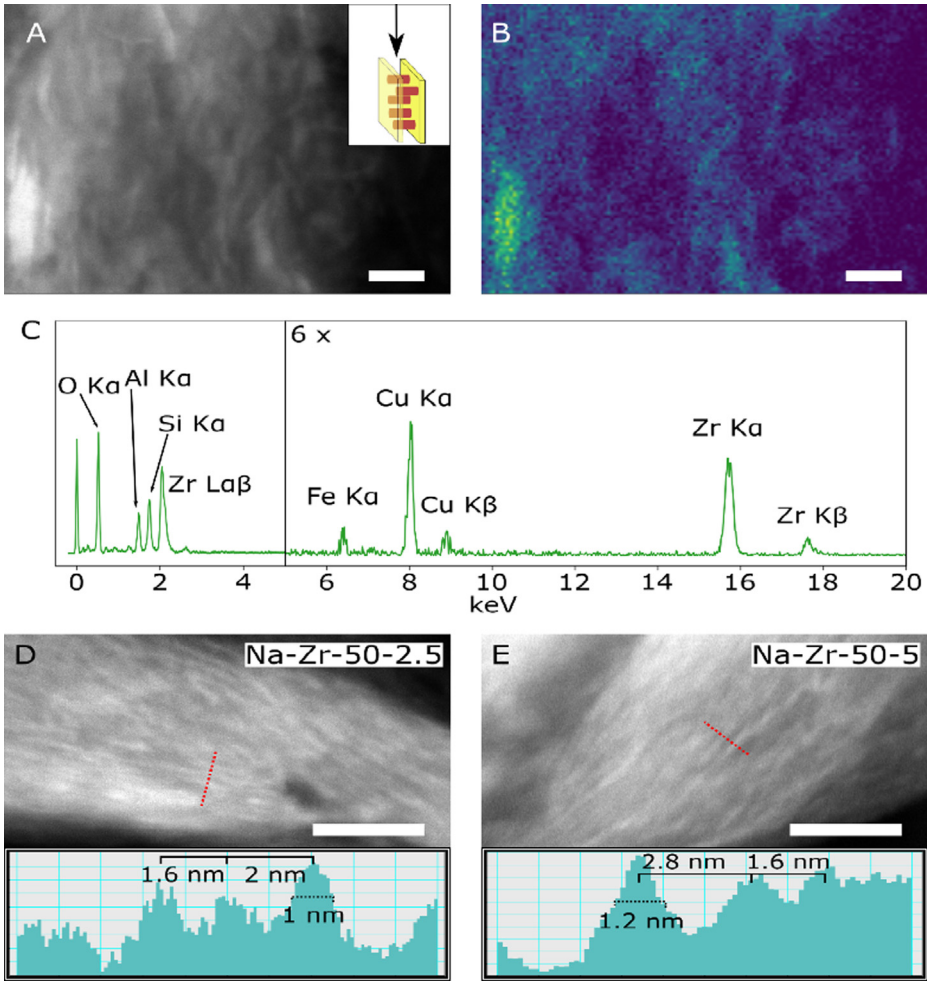

Fig. 5 The similarities between the STEM-HAADF **(A)** and STEM-EDX map of Zr-rich areas **(B)** in Zr-50-10 show that the bright fringes in the HAADF images can be correlated to areas rich in Zr. The inset in **(A)** illustrates the viewing direction, where the intercalated ZrO_2 layers are parallel to the electron beam. **(C)** The NMF-component used to construct B is dominated by Zr, but additionally contains the Al and Si from the surrounding clay. Additionally, higher resolution HAADF images of Na-Zr-50-2.5 **(D)** and Na-Zr-50-5 **(E)** with inset line profiles exemplify the relative size and spacing of the fringes. The scale bars in each image represent 20 nm.

distribution of ZrO_2 in the Na-treated samples, it was not possible to distinguish individual layers over large field-of-view at higher Zr loading (i.e., in Na-Zr-50-10). For both Na-Zr-50-2.5 and Na-Zr-50-5, the thickness of the bright layers, measured at FWHM, varied between approximately 1–2 nm. The domains were separated from peak to peak by approximately 1.5–3.0 nm. The measured layer thicknesses and separations approximately match the basal distance of the expanded clay (or a multiple of the same), indicating that the intercalation occurs at every or every second layer, which agrees with the XRD results (Fig. 1).

The hybrid, partial nature of intercalation was confirmed by basal spacing measurement using image analysis as shown in Fig. 6. As seen, the modification procedure increased the basal spacing in all samples. The distributions of basal spacing of the precursor clays were unimodal, with a mode at 1.1 nm. The modification process introduced a second mode that corresponded to intercalated layers at a basal spacing of approximately 1.5 nm. The extent of pillaring appeared to have been affected by the concentration of Zr and the type of precursor: Na-saturated clay exhibited a higher extent of pillaring and slightly longer basal spacing. The optimum concentration of Zr appeared to be 5 mmol/g – above this concentration, pillaring appeared weaker since the basal spacing distributions exhibited a weaker second mode, corresponding to intercalated layers.

Since no increased basal spacing was detected by XRD for Zr-50-10, yet some interlayer expansion was detected by HRTEM (Fig. 6), further STEM-HAADF and EDX analysis was performed. The HAADF image (Fig. 7A) shows sparse Zr-rich domains which are unevenly distributed with large separations. At larger fields-of-view, the Zr-rich domains appear in partially agglomerated structures that have no clear relation to the surrounding layered CM structure, as shown in the HAADF and EDX images (Fig. 5A, B). This lack of even, regular intercalation is consistent with the XRD results, which detects only the periodic 1 nm spacing between the CM basal planes.

The very sparse pillaring in Zr-50-10 means, however, that the separation between individual pillars is sufficient for HRTEM imaging. To determine the structure and morphology of the intercalated ZrO_2 pillars, representative HRTEM images of the precursor and Zr-intercalated clays were acquired in a viewing direction perpendicular to the clay basal planes. To better be able to distinguish individual pillars, the images were acquired at the very edges of the clay agglomer-

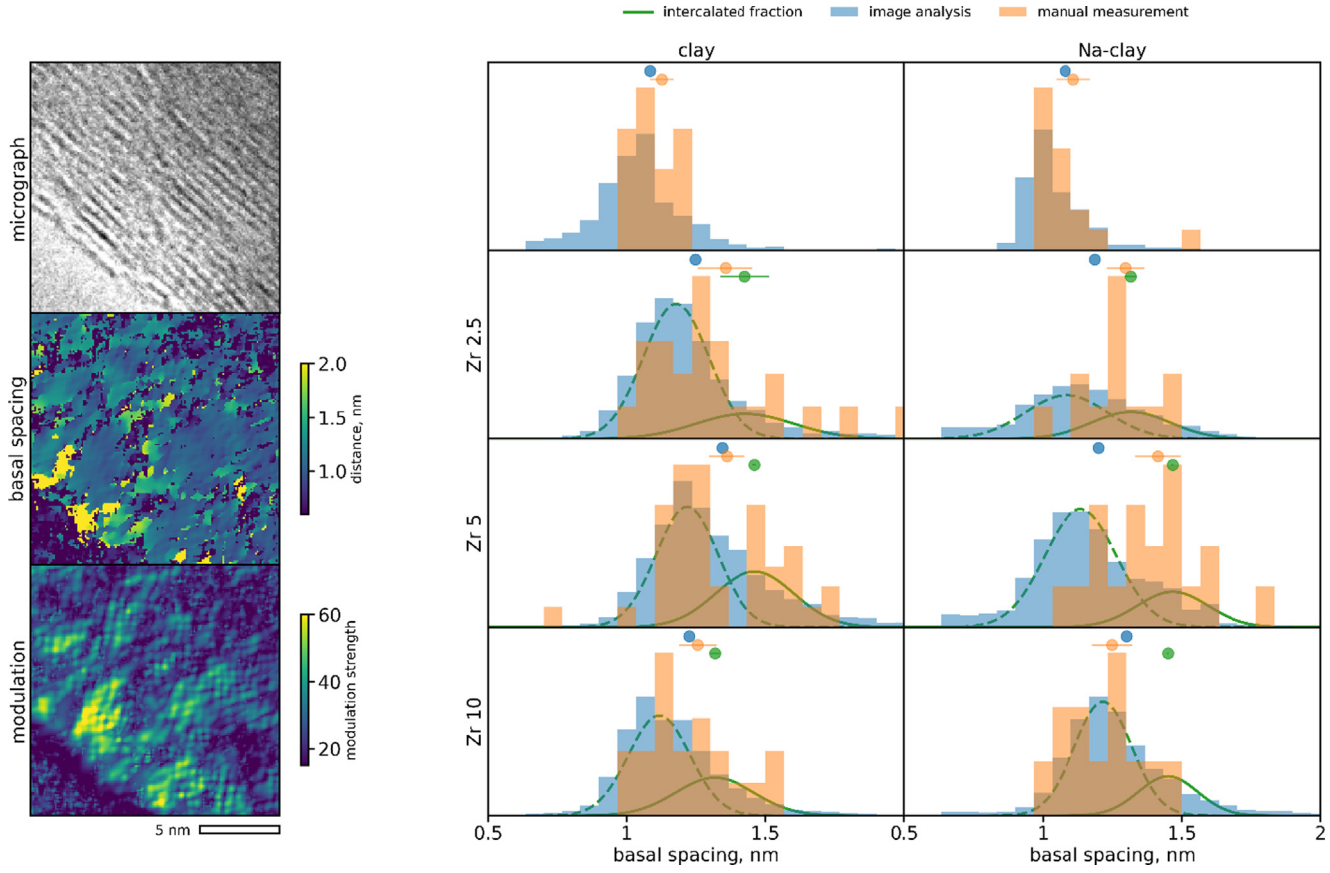

Fig. 6 Detailed analysis of basal spacing based on HRTEM imaging. The left column shows a representative HRTEM image with colour-coded maps of the basal spacing and modulation strength (measurement quality). The right column shows a matrix of basal spacing histograms obtained by manual measurement (orange) and image analysis (blue). Green curves show components of fit bimodal normal distributions to the data obtained by image analysis: the dashed curve indicates the component attributed to the precursor clay and the continuous line is attributed to the component of intercalated layers. Circles and horizontal error bars show the mean of the manual measurements (orange), the mean of the basal spacing obtained by image analysis (blue) and the mode of the component attributed to the intercalated layers (green).

ates to reduce the number of overlapping layers. Fig. 7B and C show representative images and their corresponding, radially averaged Fourier transform. The strong peak at 3.9 nm^{-1} seen in pillared samples (Fig. 7C inset) – missing from precursor materials (Fig. 7B inset) – can be attributed to the [1 1 0] reflection of tetragonal ZrO_2 (Igawa and Yoshinobu, 2001) or the

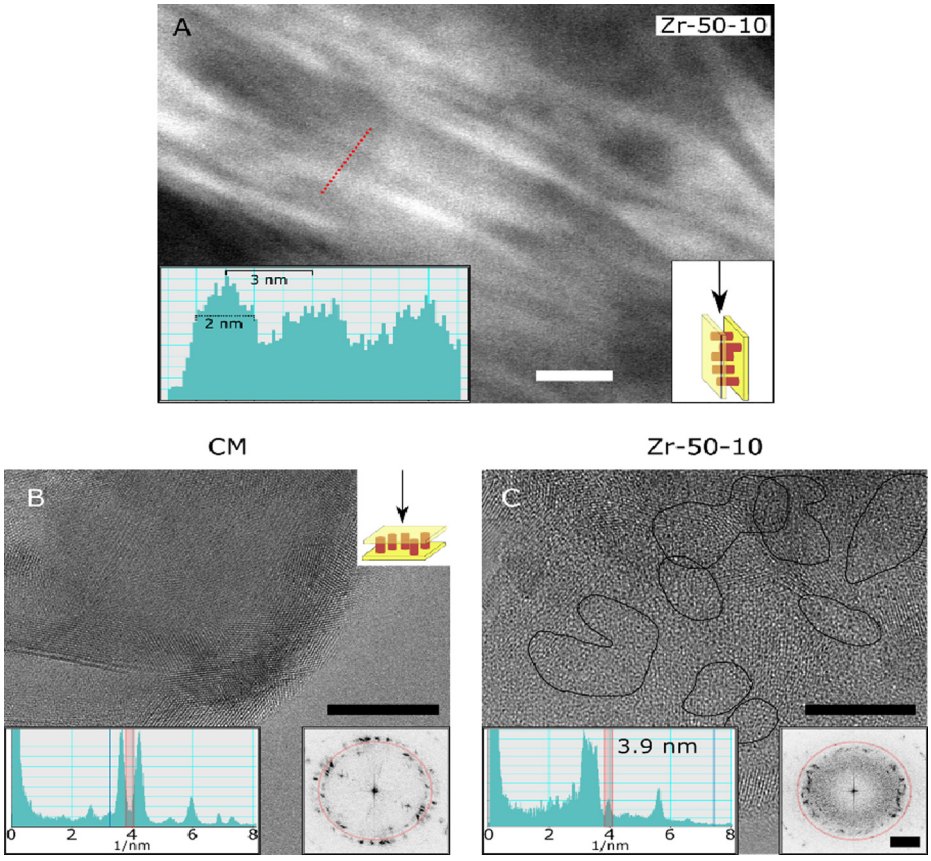

Fig. 7 HAADF image of Zr-50-10 **(A)** showing the presence of large ZrO_2-domains. Representative HRTEM images of CM **(B)** and Zr-50-10 **(C)**, both with their respective Fourier transforms and radially averaged Fourier transforms as insets, the red rectangle and circle indicating the peak at 3.9 1/nm corresponding to the [1 1 0] or [2 0 0] reflection of ZrO_2. The scale bars in images A-C correspond to 10 nm. The scale bar in the Fourier transforms insets in B-C correspond to 2 nm^{-1}.

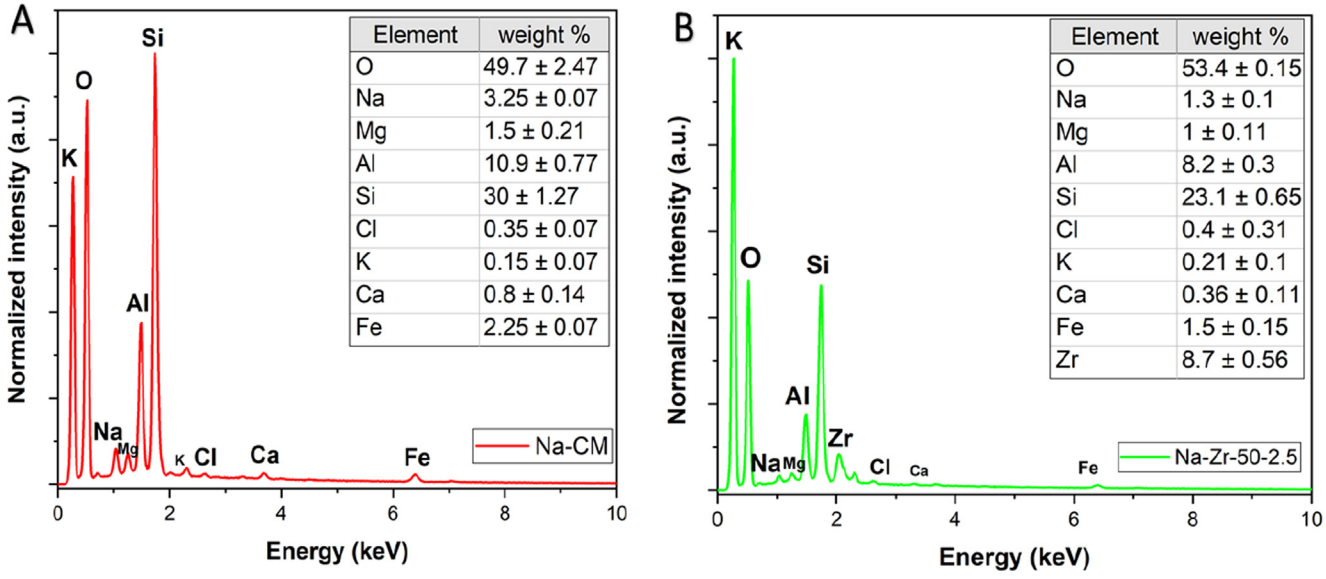

Fig. 8 EDX analysis of Na-CM **(A)** and Na-Zr-50-2.5 **(B)**.

Table 2 Elemental analysis of raw and Zr- pillared clays.

Element wt %	CM	Zr-50-2.5	Zr-50-5	Zr-50-10	Na-Zr-50-5	Na-Zr-50-10
O	50.5 ± 1.6	51.7 ± 1.40	50.3 ± 0.91	53.7 ± 0.68	49.4 ± 0.78	49.6 ± 0.58
Na	1.40 ± 0.40	0.66 ± 0.28	0.50 ± 0.21	0.90 ± 0.10	1.06 ± 0.98	0.60 ± 0.26
Mg	1.70 ± 0.30	1.10 ± 0	1.20 ± 0.05	1.10 ± 0.05	1.21 ± 0.34	0.96 ± 0.05
Al	10.9 ± 0.30	8.9 ± 0.25	9.20 ± 0.26	8.60 ± 0.20	9.20 ± 0.15	9.50 ± 0.11
Si	29.8 ± 0.30	24.16 ± 1.1	25 ± 0.30	23.2 ± 0.45	25.3 ± 0.3	26 ± 0.20
Cl	–	–	0.36 ± 0.05	0.80 ± 0	0.76 ± 0.11	0.90 ± 0
K	0.30 ± 0.17	0.20 ± 0.10	0.10 ± 0	0.10 ± 0.10	0.46 ± 0.30	0.93 ± 0.41
Ca	1.20 ± 0.30	0.17 ± 0.05	0.16 ± 0.11	0.16 ± 0.05	0.23 ± 0.05	0.16 ± 0.05
Fe	2.10 ± 0.05	1.80 ± 0.10	1.90 ± 0.05	1.60 ± 0.05	2.00 ± 0.36	2.00 ± 0.10
Zr	–	9.00 ± 0.36	10 ± 0.35	10.8 ± 0.47	8.70 ± 0.97	8.90 ± 0.17

[200] reflection of monoclinic ZrO_2. Upon filtering the images at these frequencies, distinct 5–10 nm size domains were observed, corresponding to the pillar diameter and further demonstrating the very sparse pillaring in the Zr-50–10 sample. This supports both the successful formation of crystalline ZrO_2 under the present reaction conditions and demonstrates the crucial role of the Na pre-treatment of the CM for achieving an even intercalation.

Elemental analysis of the raw and Zr- pillared clays determined by EDX is shown in Fig. 8 and Table 2. After the sodium ion exchange with raw montmorillonite (CM), the weight percentage of Na^+ ion got increased from 1.4 to 3.25%. Furthermore, the percentage content of Ca^{+2} and Na^+ ions got decreased in all the zirconium modified clays which shows that zirconium has entered into the clay structure *via* the ion exchange process.

4. Conclusion

In this work, a detailed study was carried out to investigate the effect of the precursor material (montmorillonite clay, CM, and Na-saturated montmorillonite clay, Na-CM) and concentration of zirconium on the structure of Zr-pillared clays. The obtained materials were characterized using a range of techniques. Pre-treatment of montmorillonite clay with NaCl improves the pillaring process. Better XRD and FTIR results were obtained in the case of pillared clays prepared from Na-CM which confirms the successful intercalation of zirconium in between the clay sheets. On the other hand, partial pillaring was observed in the case of CM which was further confirmed with the help of HRTEM. The concentration of zirconium also plays an important role during the process of pillaring. The lower concentration in the range of (Zr/Clay = 2.5 to 5 mmol/g) favours the process of intercalation. The dimensions and distribution of zirconium pillars created were also studied using STEM-EDX and HAADF images. The thickness of these ZrO_2 structures was found to be in the range of 1–2 nm and they were separated by a distance of 1.5 to 3 nm. The intercalation was found to be more evenly distributed throughout the material in the Na-pre-treated clay as compared to the untreated one, indicating the importance of the pre-treatment. Partial pillaring was observed in the case of CM which was further confirmed with the help of HRTEM whereby crystalline ZrO_2 domains were observed. Zr-PILCs showed high specific surface area, porosity, and thermal stability as compared to precursor material. The development of these nanoporous clay-based materials has great application in the field of material science. The porosity and specific surface area of these materials can be tuned so that they can be used as catalysts or adsorbents. There are numerous interesting areas where the application of these materials has not yet been explored such as the elimination of nutrients or biological pathogens from wastewater.

Declaration of Competing Interest

The authors declare that they have no known competing financial interests or personal relationships that could have appeared to influence the work reported in this paper.

Acknowledgements

This research was supported by the European Union and the Hungarian Government in the framework of the GINOP 2.3.4-15-2016-00004 project. Zoltán Németh would like to thank the Bolyai János Research Scholarship Program. Martin Ek and David Wahlqvist acknowledge funding from the Swedish Research Council (2017-04902).

Appendix A. Supplementary data

Supplementary data to this article can be found online at https://doi.org/10.1016/j.arabjc.2022.103706.

References

Ammann, L., Bergaya, F., Lagaly, G., 2005. Determination of the Cation Exchange Capacity of Clays with Copper Complexes Revisited. Clay Miner. 40 (4), 441–453. https://doi.org/10.1180/0009855054040182.

Bačić, I. et al, 2017. Thermal and Structural Studies of Sol–Gel-Derived Yttria-Doped ZrO2 Nanoparticles: Effect of Annealing Condition. J. Therm. Anal. Calorim. 127 (1), 197–206. https://doi.org/10.1007/s10973-016-5904-x.

Baloyi, J., Ntho, T., Moma, J., 2019. Synthesis of Highly Active and Stable Al/Zr Pillared Clay as Catalyst for Catalytic Wet Oxidation of Phenol. J. Porous Mater. 26 (2), 583–597. https://doi.org/10.1007/s10934-018-0667-3.

Bergaya, F., Aouad, A., Mandalia, T., 2006. Chapter 7.5 Pillared Clays and Clay Minerals. Developments in Clay Science 1, 393–421. https://doi.org/10.1016/S1572-4352(05)01012-3.

Barrer, M., Macleod, D.M., 1955. Activation of Montmorillonite by Ion Exchange and Sorption Complexes of Tetra-Alkyl Ammonium Montmorillonites. Transactions of the Faraday Society 51, 1290–1300. https://doi.org/10.1039/TF9555101290.

Bertella, F., Pergher, S.B.C., 2017. Scale up Pillaring: A Study of the Parameters That Influence the Process. Materials 10 (7), 1–12. https://doi.org/10.3390/ma10070712.

Brindley, G.W., Sempels, R.E., 1977. Hydroxy-Aluminium Beidellites. Clay Miner. 12, 229–237. https://doi.org/10.1180/claymin.1977.012.3.05.

Burch, R., Warburton, C.I., 1986. Zr-Containing Pillared Interlayer Clays. I. Preparation and Structural Characterisation. J. Catal. 97 (2), 503–510. https://doi.org/10.1016/0021-9517(86)90021-7.

Chae, H.J., Nam, I.S., Ham, S.W., Hong, S.B., 2001. Physicochemical Characteristics of Pillared Interlayered Clays. Catal. Today 68 (1–3), 31–40. https://doi.org/10.1016/S0920-5861(01)00320-0.

Chauhan, M., Saini, V.K., Suthar, S., 2020. Removal of Pharmaceuticals and Personal Care Products (PPCPs) from Water by Adsorption on Aluminum Pillared Clay. J. Porous Mater. 27 (2), 383–393. https://doi.org/10.1007/s10934-019-00817-8.

Cool, P., Vansant, E.F., 1998. Pillared Clays : Preparation, Characterization and Applications. In: Synthesis. Molecular Sieves (Science and Technology), 1. Springer, Berlin, Heidelberg.

Frost, R.L., Huada Ruan, J., Kloprogge, T., Gates, W.P., 2000. Dehydration and Dehydroxylation of Nontronites and Ferruginous Smectite. Thermochimica Acta 346 (1–2), 63–72. https://doi.org/10.1016/S0040-6031(99)00366-4.

Gand, L.M., Vicente, M.A., Gil, A., 2000. Preparation and Characterization of Manganese Oxide Catalysts Supported on Alumina and Zirconia-Pillared. Clays 196, 281–292. https://doi.org/10.1016/S0926-860X(99)00479-2.

Gil, A., Korili, S.A., Trujillano, R., Vicente, M.A., 2011. A Review on Characterization of Pillared Clays by Specific Techniques. Appl. Clay Sci. 53 (2), 97–105. https://doi.org/10.1016/j.clay.2010.09.018.

Gil, A., Vicente, M.A., 2020. ScienceDirect Progress and Perspectives on Pillared Clays Applied in Energetic and Environmental Remediation Processes. Curr. Opin. Green Sustainable Chem. 21, 56–63. https://doi.org/10.1016/j.cogsc.2019.12.004.

Igawa, N., Yoshinobu, I., 2001. Crystal Structure of Metastable Tetragonal Zirconia up to 1473 K. J. Am. Ceram. Soc. 84 (5), 1169–1171. https://doi.org/10.1111/j.1151-2916.2001.tb00808.x.

KouSun, M.R., Mendioroz, S, Guijarro, M.I., 1998. A Thermal Study of Zr-Pillared Montmorillonite. A Thermal Study of Zr-Pillared Montmorillonite 323 (1–2), 145–157, Thermochim. Acta. doi: https://doi.org/10.1016/S0040-6031(98)00540-1.

Lin, J., Jiang, B., Zhan, Y., 2018. Effect of pre-treatment of bentonite with sodium and calcium ions on phosphate adsorption onto zirconium-modified bentonite. J. Environ. Manage. 217, 183–195. https://doi.org/10.1016/j.jenvman.2018.03.079.

Madejová, J., 2003. FTIR Techniques in Clay Mineral Studies. Vib. Spectrosc. 31 (1), 1–10. https://doi.org/10.1016/S0924-2031(02)00065-6.

Mnasri-ghnimi, S., Frini-srasra, N., 2019. Applied Clay Science Removal of Heavy Metals from Aqueous Solutions by Adsorption Using Single and Mixed Pillared Clays. Appl. Clay Sci. 179, 105151. https://doi.org/10.1016/j.clay.2019.105151.

Muto, S., 2019. Non-Negative Matrix Factorization and Its Extensions for Spectral Image Data Analysis. e-journal of Surface Science and Nanotechnology 17, 148–154. https://doi.org/10.1380/ejssnt.2019.148.

Najafi, H. et al, 2021. A Comprehensive Study on Modified-Pillared Clays as an Adsorbent in Wastewater Treatment Processes. Process Saf. Environ. Prot. 147, 8–36. https://doi.org/10.1016/j.psep.2020.09.028.

Onyango, Maurice, S., Dalibor, Kuchar., Mitsuhiro, Kubota., Hitoki, Matsuda., 2007. Adsorptive Removal of Phosphate Ions from Aqueous Solution Using Synthetic Zeolite. Ind. Eng. Chem. Res. 46 (3), 894–900. doi:https://doi.org/10.1021/ie060742m.

NerisMeireles, A., Jailson Machado Ferreira, Gardennia Fonseca, M., Ieda Maria Garcia dos Santos, 2020. Undoped Tetragonal ZrO2 Obtained by the Pechini Method: Thermal Evaluation of Tetragonal–Monoclinic Phase Transition and Application as Catalyst for Biodiesel Synthesis. Journal of Thermal Analysis and Calorimetry (0123456789). https://doi.org/10.1007/s10973-020-09286-7.

Toth, P., 2021. Nanostructure Quantification of Turbostratic Carbon by HRTEM Image Analysis: State of the Art, Biases, Sensitivity and Best Practices. Carbon 178, 688–707. https://doi.org/10.1016/j.carbon.2021.03.043.

Uddin, M.K., 2017. A Review on the Adsorption of Heavy Metals by Clay Minerals, with Special Focus on the Past Decade. Chem. Eng. J. 308, 438–462. https://doi.org/10.1016/j.cej.2016.09.029.

Valenzuela, M.A., Lara, V.H., Bosch, P., 2003. Effect of Microwave Irradiation Time on the Synthesis of Zirconia-Pillared Clays. Materials Letters 57 (5–6), 1220–1223. https://doi.org/10.1016/S0167-577X(02)00961-8.

Vaughan, David E.W., Roger J. Lussier, John S. Magee Jr., 1979. U.S. Patent No. 4,176,090. "Pillared Interlayered Clay Materials Useful as Catalysts and Sorbents." (19).

Yamanaka, S., 1979. High Surface Area Solids Obtained by Reaction of Montmorillonite with Zirconyl Chloride. Clays Clay Miner. 27 (2), 119–124. https://doi.org/10.1346/CCMN.1979.0270207.

Yuan, P. et al, 2008. A Combined Study by XRD, FTIR, TG and HRTEM on the Structure of Delaminated Fe-Intercalated/Pillared Clay. J. Colloid Interface Sci. 324 (1–2), 142–149. https://doi.org/10.1016/j.jcis.2008.04.076.

Zhang, L. et al, 2014. Hydration and Mobility of Interlayer Ions of (Nax, Cay)-Montmorillonite: A Molecular Dynamics Study. J. Phys. Chem. C 118 (51), 29811–29821. https://doi.org/10.1021/jp508427c.

Zhang, T. et al, 2020. Removal of Heavy Metals and Dyes by Clay-Based Adsorbents: From Natural Clays to 1D and 2D Nano-Composites. Chem. Eng. J. 127574. https://doi.org/10.1016/j.cej.2020.127574.

Zhou, C., Dongshen Tong, Weihua Yu, 2019. Nanomaterials from Clay Minerals: A New Approach to Green Functional Materials Smectite Nanomaterials: Preparation, Properties, and Functional Applications. Elsevier Inc. https://doi.org/10.1016/B978-0-12-814533-3.00007-7.

Zhou, J. et al, 2010. Polymeric Fe / Zr Pillared Montmorillonite for the Removal of Cr (VI) from Aqueous Solutions. Chem. Eng. J. 162 (3), 1035–1044. https://doi.org/10.1016/j.cej.2010.07.016.

Zou, Y. et al, 2020. Strong Adsorption of Phosphate from Aqueous Solution by Zirconium-Loaded Ca-montmorillonite. Appl. Clay Sci. 192, 105638. https://doi.org/10.1016/j.clay.2020.105638.

Zviagina, B.B., Drits, V.A., Dorzhieva, O.V., 2020. Distinguishing Features and Identification Criteria for K-Dioctahedral 1M Micas (Illite-Aluminoceladonite and Illite-Glauconite-Celadonite Series) from Middle-Infrared Spectroscopy Data. Minerals 10 (2), 1–27. https://doi.org/10.3390/min10020153.